Development of a TEGIC-Detector for Heavy Ions

BACHELOR THESIS

STEFFEN MAURUS

24. AUGUST 2012

TECHNISCHE UNIVERSITÄT MÜNCHEN

first reviewer: Prof. W. Henning
second reviewer: Prof. P. Böni
scientific supervisor: Dr. R. Gernhäuser

Abstract

To satisfy the future requirements for high rate heavy ion-experiments, new concepts of faster gas-detectors have to be invented and tested experimentally. These high rate-chambers are very important to detect the atomic number by an energy loss measurement or to determine the trajectories of ionising particles.

A promising concept to increase the counting rate capabilities of ionisation chambers is the tilted-electrode-gas-ionisation-chamber (TEGIC) with a series of plane electrodes tilted with respect to the beam axes.

In the framework of this thesis a construction concept of a TEGIC-prototype was developed, realized and a full scale prototype was built. In addition an experimental test was performed at the MLL Tandem-accelerator in Garching using a 40 MeV ^{7}Li and a 20 MeV proton beam. A systematic sutdy of the energy loss in different segments of the detector showed the typical Bragg curve for stopped particles. Even at particle rates above 130 kHz the detector showed only a minor degradation in energy resolution which was still limited by the beam properties and not by the detector with a value of ΔE$<$15keV $\cdot$ 2.35.

In addition effects were investigated when the incoming beam not perfectly hits the center of the final detector prototype. As a result a minimum active area of 2.8 x 8 cm^2 was determined.

Contents

Chapter 1

Introduction

Gas-Ionisation-Chambers have become a very important part in the study of ionisation radiation. The field of application is very wide spreading, from small devices like the Geiger-Counter for the simply detection to very big application like A.L.I.C.E. for the detailed measurement of ionisation particles.

From simple counter chambers they undergone a significant progress to complex detectors, which can determine the energy and charge of the ions, to identify unknown fragments. After years it is even possible to reconstruct the trajectory of the particles using the Time-Projection technique with a precision of a few micron.

Especially for the usage in high radiation environment the detectors have the advantage that the active material does not take damage through the ionisation particles, in contrast to semiconductor detectors because of the steady replacement of the detector gas. In addition it is easier and cheaper to build especially large area gas ionization chamber instead of another detector type, because no complicated crystal growth or expensive semi conductor technique is required.

Due to the limited drift velocity of charge carriers in a detector gas these detectors have a typical rate limitation per detector element. Especially in case of ionisation chambers for heavy ions, where the energy loss of the particles has to be measured very precisely, this introduces a severe limitation.

In modern secondary beam experiments using particles very far off the valley of stability the requirement for high rate detectors is more important than in the past. Through new particle accelerators and large acceptance fragments seperators the detectors are reaching their limit of operation. To satisfy these new requirements a new concept was invented, the Tilted-Electrode-Gas-Ionisation-Chamber (TEGIC) [1], to provide a higher detection rate. This concept and the design and fabrication of a TEGIC prototype and additionally the experimental test are discussed in the framework of this bachelor thesis.

Chapter 2

Basic Concept

2.1 Ionisation Process

The energy loss of a charged particle traveling through a material can be described primarily through the Coulomb interaction between this particle and the electrons in the material as well as with the positive nuclei.
Because of the rather small radii of the nuclei in comparison with the radii of the whole atoms, the interaction with the electrons is much more important for high energy particles.

As the incident particle interact through the Coulomb force, it transfers its energy to the bound electrons by inelastic scattering. Depending on the transferred energy this could result in an ionisation or an excitation of the bounded electron. Let's focus the further discussion on the case of an atomic gas.
To ionize the atom the electron must gain enough energy to overcome the ionisation potential. Its final kinetic energy is the difference between the transferred energy and the ionisation potential. If the transferred energy is less than this potential, the electron gets excitation and after a short time it emits a photon or transfers energy by inelastic scattering to falls back to the ground state.
The incident charged particle interacts with many of electrons simultaneously. The Bethe-Bloch Formula provides a good description of the average energy loss of a particle with charge Z and velocity $\beta = \frac{v}{c}$ over a wide range of energies. [2, p.97ff.]

$$\frac{dE}{dx} = \frac{4 \cdot \pi \cdot N \cdot e^4 \cdot Z^2}{m \cdot c^2 \cdot \beta^2} \left(ln \frac{2 \cdot m \cdot c^2 \cdot \beta^2 \gamma^2}{I} - \beta^2 \right) \tag{2.1}$$

([3, p. 29]) Here m is the electron mass, c the vacuum speed of light, $\gamma^2 = \frac{1}{(1-\beta^2)}$ the Lorenz factor, N is the density of electrons in the material and I is the mean excitation energy of the atoms in the stopping Material. This formula is only valid for heavy ions and not for electrons or positrons. [3, S.29]
The energy loss of a charged particle as it flies through the material is not linear. The correlation between the energy loss and the distance can be described by a Bragg curve, as it is illustrated for a 5.49 MeV α particle in figure 2.1.
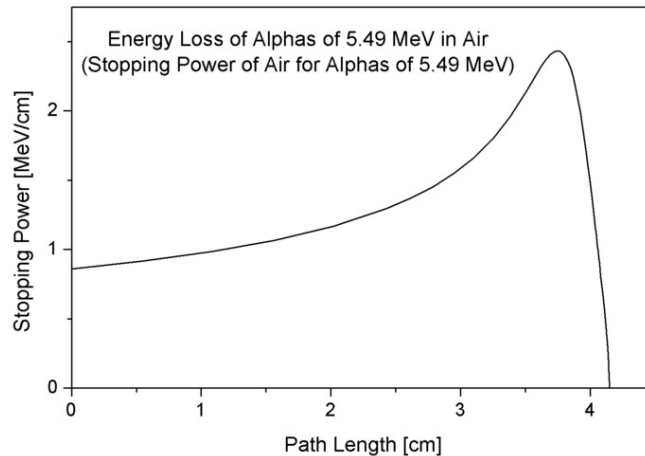
Figure 2.1: non-linear energy-loss for a 5.49 MeV α particle in air with a maximum (bragg peak) shortly before the ion stoppes. [4]

The maximum deposited energy per unit length of the charged particle occurs shortly before the ion gets stopped. This peak is called Bragg-Peak, introduced by the $\frac{1}{\beta^2}$ term in equation 2.1.

2.2   Ionisation Chamber

The most simple principal gas ionization chamber layout consists of two parallel electrodes on a different potential, leading to an electric field. Other geometries like cylindrical segmented or more complicated chambers are also used.

Between the electrodes is the detection gas, where the incident particle loose energy by producing electron-ion pairs. So the detector uses the effect of ionisation to detect or track these particles.

The typical energy that is necessary to produce an electron-ion pair is in the order of 25-45 eV depending on the detector gas. [5] This energy is sometimes a factor 2 higher than the ionisation energy of the material, because it consideres interactions with electrons that lead to excitation, where the incident charged particle looses energy, but no electron-ion pair is produced. This means e.g. a particle will produce approximately 38 000 electrons when it deposit 1 MeV of kinetic energy in Argon detector gas. The direct ionisation produced by incident particle is called primary ionisation. Secondary ionisation can occur when the electrons gained enough kinetic energy from the electric field to ionise other nuclei. This process is not discussed in the framework of this bachelor thesis, as this affect occur in proportional counters and not in ionisation chambers.

After the ionisation the electron and the positive nuclei are attracted by the external electric field. The electron moves to the positive charged anode in contrast to the resulting motion of the positive nuclei which drifts to the negative charged cathode. The basic idea is illustrated in figure 2.2.
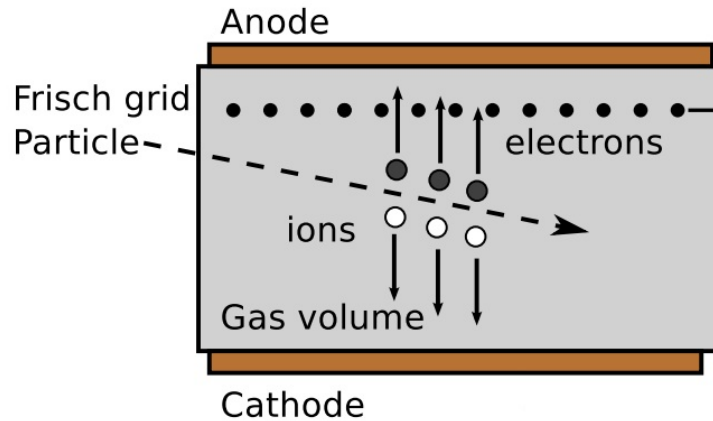
Figure 2.2: The basic idea of the ionisation chamber with a incident beam and the ionisation path. The electrons drift to the positive anode and the ions to the negative cathode. [6]

The same amount of force is acting on both particles as $\vec{F} = \vec{E} \cdot q$. The resulting drift velocity of the electron and the ion is equal to $V_{drift} = \frac{\mu \cdot \vec{E}}{p}$ where p is the pressure of the gas an μ is the mobility. This mobility is different by a factor of 1000 between e$^-$ and the ion. For a typical detector the time that the electron needs to reach the anode is about 1 μs in contrast to the positive charged ion which moves about a thousand times slower. [2, p143f]

The time which the electrons need to reach the anode is also the limiting factor for the counting rate. If two particles reach the detector without enough time lag between them only a combination of both signals is measured. The problem occurs when the electrons produced by the first ionizing particle not yet reached the anode and the second particle is already ionizing other atoms, as the readout electronic integrates 1 μs (charge collection time) to get enough resolution. So the detector sees only the sum of the energy losses of both particles and is unable to resolve every single event. This effect is called pile-up and is a feature of the electronics. If the setting of the charge collecting or shaping time is too long the chance of measuring a pile-up increases. Is this setting too short only a fraction of the signal procuded by the electrons gets measured with negative effects for the resolution. The problem is illustrated in figure 2.2.
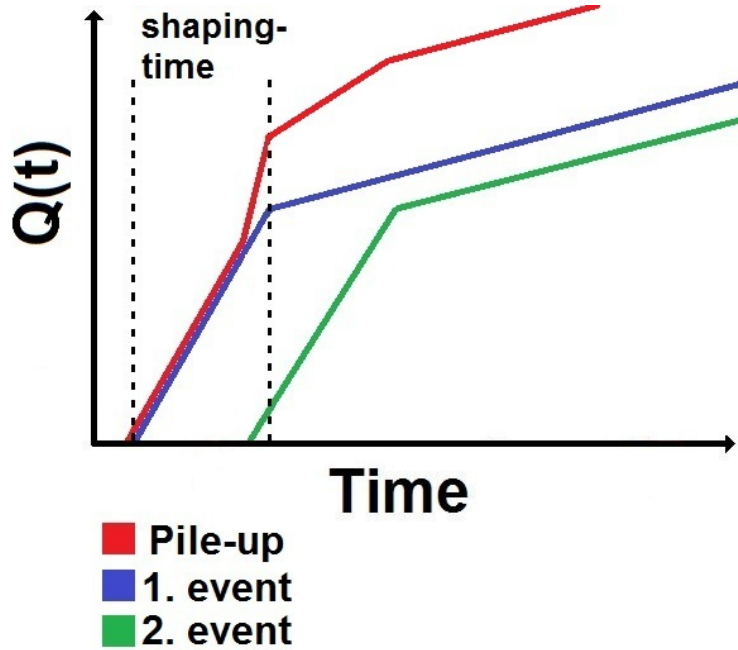
Figure 2.3: Two ionising particle reach the detector without enough time lag. Only the sum of the energy loss is measured. The Information of every single event is lost.

As only the sum of both energy losses is measured, the information of every single energy loss is lost. It is also unable to reconstruct the trajectory of every single particle. If the electrons need 1 μs to reach the anode, the problem could occur at particle rates higher than 100 kHz. To suppress this effect the Frisch grid was invented. This grid is between the anode and cathode as illustrated in figure 2.2. The function of this grid is to shield the anode from the signal generated by the slow ions and electrons between the grid and the cathode. Consequently only charged particles between the grid-anode gap will produce an output signal.

But there is also a possibility that even this upgrade isn't able to resolve every event. If two ionising particles reach the detector at the same time but different positions, problems could occur, as the detector need 1 μs of integration time. So the electrons of the second event reach the Frisch grid before the integration is completed and again the sum is measured

2.3   TEGIC-Upgrade

One solution to overcome the problem discussed in the end of section 2.2 is the tilted electrode gas ionisation chamber (TEGIC). To decrease the time that the electrons need to drift to the anode the electrodes are mounted close to 90° with respect to the beam axis. So the drift distance which is still the distance between anode and cathode (see figure 2.4) could be shorter in comparison to a normal detector shown in figure 2.2 what effects the counting rate in a positive way.

At an angle of 90° the applied electrical field is parallel to the beam and the produced ions and electrons wouldn't be separated or they pass each other as they drift through the detector gas. Depending on the details of the geometry electrons and ions cross each other's way and additional recombination might occurrs for the electrons by the slow ions, what effects the measured signal of the detector. A further effect is the modification of the electric field that would cause a shift in the drift velocities of the electrons and ions.
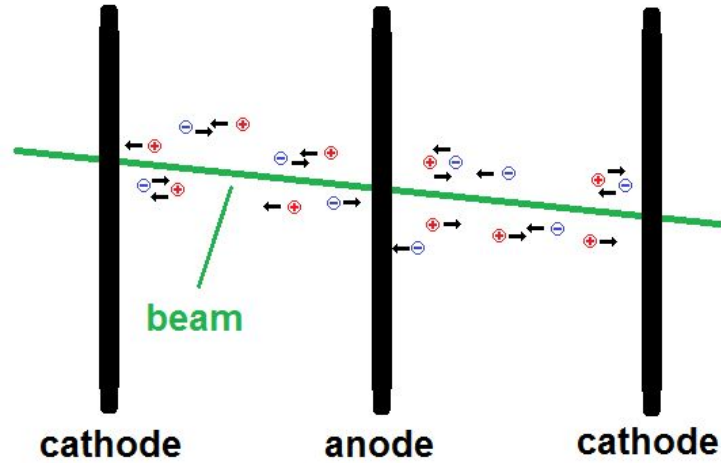
Figure 2.4: Problems that occur if the electrodes are perpendicular related to the beam: Modification of the electric field with impact on the drift velocities and a increasing number of recombination processes.

Both effects overcome by the electrodes tilted relatively to the beam axis. To provide a long ionisation distance for the incoming particle and therefore a high energy loss, many anode-cathode pairs are mounted directly behind each other as pictured in figure 2.5.
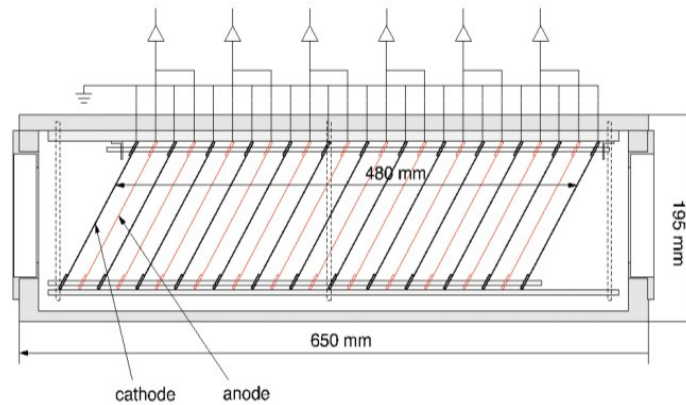

Figure 2.5: Principle of the TEGIC detector with tilted electrodes relatively to the horizontal beam axis [1]

As every anode could be read out individually the energy loss per segment is measured similar to the concept of a Multi Sampling Ionisation Chamber (MUSIC) [7] To 'amplifie' signals with a low deposited energy, several anodes could be connected to each other with a bigger resulting signal, as the drift path increases and therefore more charges can be collected.
A disadvantage of this concept is the energy loss of the incoming ionising particle as they pass through the electrodes that can't be measured. So a fraction of the kinetic energy "disappears" and the reconstruction of the initial kinetic energy gets more difficult. This was an important effect for the test experiment discussed in chapter 4 which is not of interest in its final application for the identification of high energy heavy ions which easily pass a few $\frac{g}{cm^2}$ of material.

2.4   Properties of Ionisations Chambers

2.4.1   Pulse Formation

In this section the shape of the measured signal for a parallel-plate ionisation chamber will be discussed. As illustrated in figrue 2.4.1 the detector consists of two parallel plates with a capacity C and a parallel resistor R. V(t) represents the measured read out signal and V_0 the applied voltage on the detector plates. X_0 is the distance to the anode at which one ion-electron pair is produced by the incoming ionising particle.
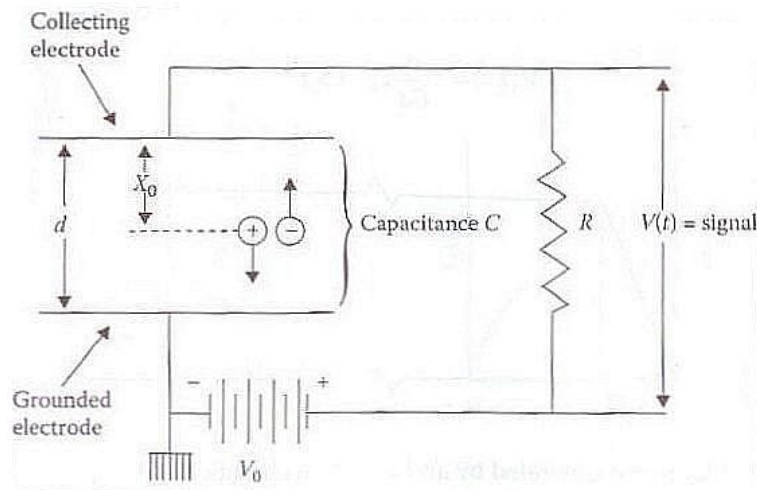

Figure 2.6: Schematic layout of a parallel plate detector. C is the capacity of the detector with apllied voltage V_0. Togehter with the parallel resistor they form a RC circiut.[2, p147]

The resulting function V(t) splits into two parts as the electrons reach the anode at time T^- and the much slower ions at time T^+, what causes distinct singals at the output. The discussion of the function V(t) is in the attachment A.4.

$$V(t) = \begin{cases} -\frac{e}{Cd}\left(\omega^- + \omega^+\right)t & \text{for } 0 < t \leq T^-\text{and } T^- < T^+ \\ -\frac{e}{Cd}\left(x_0 + \omega^+ t\right) & \text{for } T^- < t < T^+\text{and } T^- < T^+ \end{cases}$$

The Voltage changes linear with time. As the velocity of the electrons is much faster than the velocity of the ions, V(t) increases very fast till the electrons reaches the anode in the most likely case that $T^-{<}T^+$. Then the function increases slowly, till also the ions reach the cathode and V(t) reaches the maximum of $V(T^+) = -\frac{e}{C}$. After both particles have reached the electrodes, the voltage will decay with a decay constant RC. The function is plotted in figure 2.4.1.
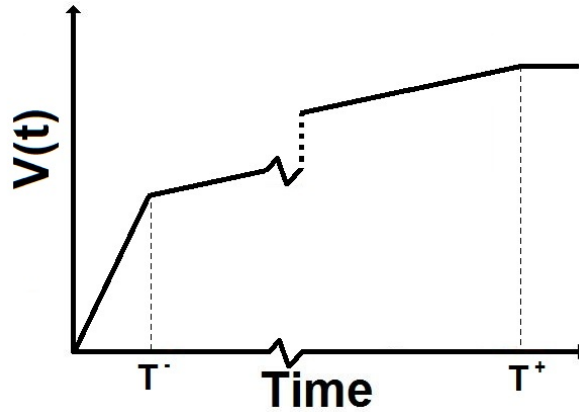
Figure 2.7: V(t) plottet against the time. T^- is the time electrons need to reach the anode, T^+ the time ions need to reach the cathode.

The real pulse generated by the electrons and the ions look a little bit different, because not all electron-ion pairs are procuded at x_0. As the ionisation is produced along the trajectory of the incident particle the resulting pulse is a superposition of all electrons and ions with different time constants T^- and T^+. As a result the sharp edge at T^- will disappear and the whole function gets smoother. In reality also a 'chop off' technique is used, because the decay time of the pulse is to long, so only the signal part generated by the electrons is used for the readout while the ionic part being about a factor 1000 slower is chanceled by the electronics. [2, p147 ff]

2.4.2 Drift Velocity in Detector Gases

Without any applied electric field there is no net velocity in the motion of the ions and electrons. They will move randomly through the gas colliding with other particles or recombined by emitting a photon. With an applied electric field there is a net velocity, that made it possibly to separate the electrons from the positive ions and collect them at the electrodes. In order to measure as many events per second as possible, the velocity of the electrons must be as fast a possible and constant for a constant signal shape. Figure 2.4.2 shows the correlation between the pressure normalized electric field ($\frac{V}{m}$) and the net electron velocity for a gas mixture of 90 % Argon and 10 % Methane in comparison with pure methane.

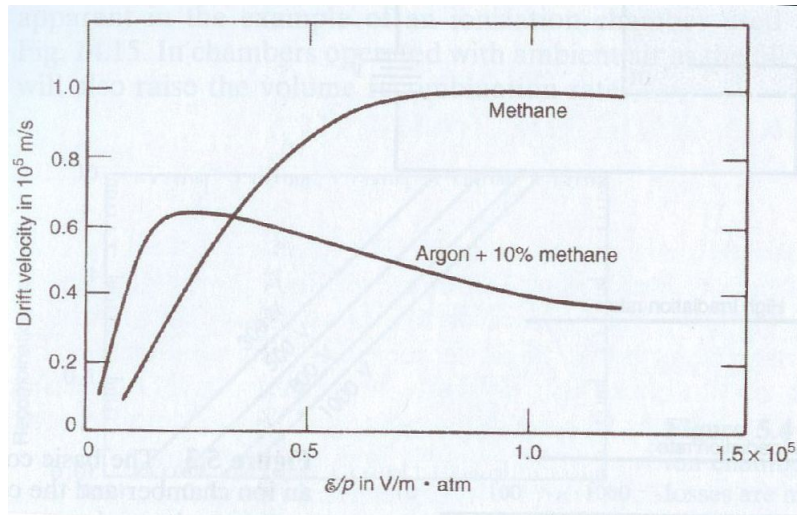**Figure 2.8:** The drift velocity of the electrons plotted vs the pressure normalized electric field.

The net velocity does not increase linear with the applied electric field. For most gas mixture there is a point of the maximum velocity. If the electric field is stronger than the value of this maximum, the net velocity decreases due to the velocity dependence of the scattering cross section in different material. [5]

Chapter 3

A TEGIC-Prototype Detector

After the principal idea of the Tilted Electrode Foil Gas Ionisation Chamber was introduced in the last chapter, the general mechanic layout, the foil mounting and the electronics readout are discussed in the following sections.

3.1   Mechanical Structure

There are two important aspects in the detector layout which directly affect the signal and resolution of the final device.

While the influence of gas purity will be discussed in chapter 3.2, especially the mechanical precision is the most important constraint on the detector resolution. If the electrodes are not equally separated or the angle with respect to the beam is not precisely constant in all foils, the effective length of the individual detector cells become position dependent and different for each of the consecutive cells. This affects the resolution of the detector and also requires a position dependent calibration.

To distinguish two atoms, which differ in one atomic number, a maximum variance of 1.2 mm for the space between the electrodes is allowed (see attachment A.3). Because of the techniques that were used to produce the prototype, a calculated uncertainty of 0.45 mm could be provided. This uncertainty is made of the impreciseness of the side panels with a value of 0.2 mm (8 mil) and a tolerance of 50 μm for the connectors. In addition a further uncertainty arise through the soldering of the connectors with approximately 0.2 mm.

3.2   Housing

The mechanical layout of the prototype detector developed in the framework of this thesis is based on a gas tight housing that encloses 17 tilted electrodes, which consist of a PCB frame covered with 2 μm aluminized Mylar$^{®}$ foils [1] and a gas distribution system to provide a smooth gas exchange every 30 minutes in the hole active volume.

The main structure of the housing consists of a rather large [2] ready made aluminium strand casting profile. This allows for a quite fast and easy making, a modular concept and intrinsic gas tightness, on the cost of a limited flexibility in the geometrical dimensions.

Especially the gas tightness is very important. Gas impurity can have a huge impact on the drift times of the electrons. Another problem could arise, when the intruded gas has a very

---

[1]Mylar$^{®}$ from DuPont
[2]Dimensions in mm: 120x200x310 with 6 mm wall thickness

huge electron affinity, which would trap parts of the electrons. Furthermore a non stable gas mixture would change the resolution of the detector with time. For a homogeneous gas flow throughout the whole chamber and regular gas exchange a curved stainless metal tube [3] with nine gas leaks (distance 3 cm) was attached to both, the bottom and the top wall inside of the housing. The outer tubing was connected via a standard flexible line to the gas supply.

For the construction it was necessary to have access to the inside of the housing. Therefore the side walls were removable. This was realised with printed circuit boards (PCB) which are quasi metal plates that are easier to fabricate and mechanically very precise. The housing and the PCB were fixed together with M2 screws. As it had to be gas tight, a flat 0,5 mm Viton$^{®}$ [4] sealing was put between the two parts. To provide a good gas tightness and electrical shielding the distance between neighbouring screws was 2 centimetres, with a total number of 42 per side wall.

As a requirement the entrance and exit window must provide both a thin barrier for the ions and gas tightness. Because of that a 2μm Mylar$^{®}$ was glued with epoxy resin to the 6 mm edge of the aluminium profile. Thus the sides of the detector box are very sensitive. The final housing is pictured in figure 3.1.
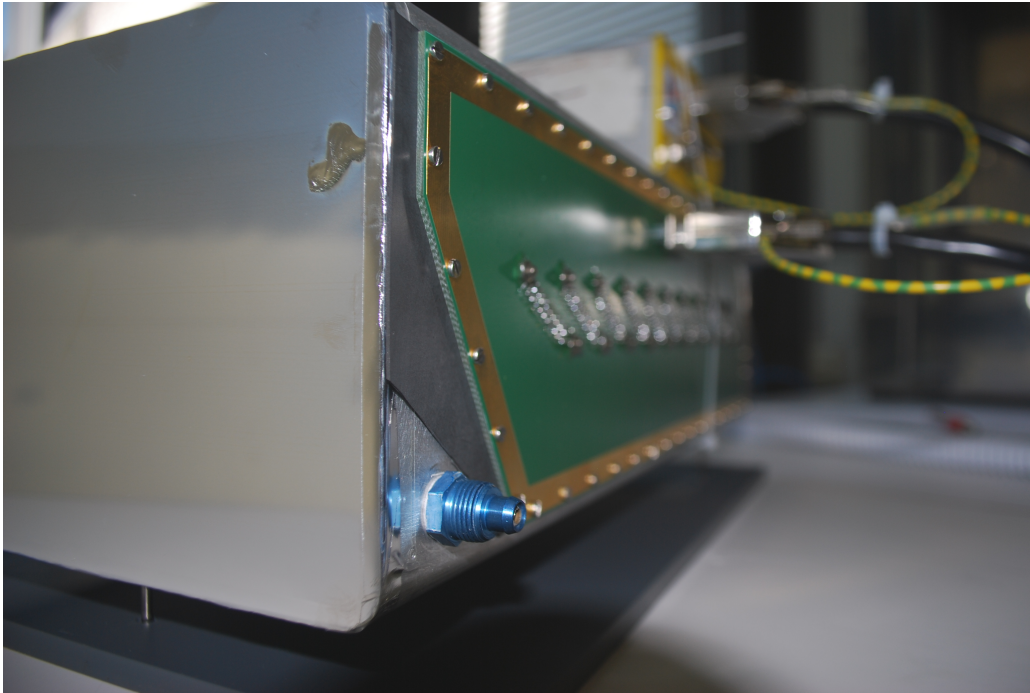

Figure 3.1: Ready-made detector housing. The detector entrance window on the left was nicely stretched to provide a homogenious thickness for the ions passing. The picture allows a clear view on the gas inlet (blue connector) the side PCB (green) and the Viton sealing.

---

[3]300x5 mm^2 with 2.5 mm wall thickness

[4]Viton$^{®}$ from DuPont

3.3 Printed Circuit Boards

The mechanical layout for the frames of the detector foils (electrodes) and their mounting where realised by printed circuit boards. The advantage of this layout is a variable and very precise structure. Especially for the foil frame where 32 units had been produced during the development the technique had turned out to be fast and cost effective.

3.3.1 Side Panel

The side panel is primarily a copper plate with solder resist and a gold-coated frame which provides a flat seal-surface. To purchase only one type of PCB for the left and right side panel, a rather symmetric layout was used on top and bottom layer, so that the PCB could be mounted in the same direction on both sides. To make this design easier to understand, figure 3.2 shows the readout panel and a detailed look of the top and bottom layer. Figure 3.3 shows the side panels with mounted electrodes but without the detector housing.
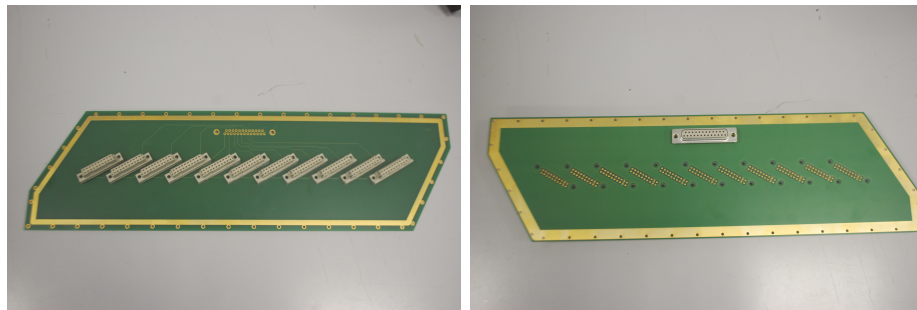

Figure 3.2: Top and bottom of the side panel. On the left side the inner surface with the electrode connectors and on the right the outside with the signal output connector
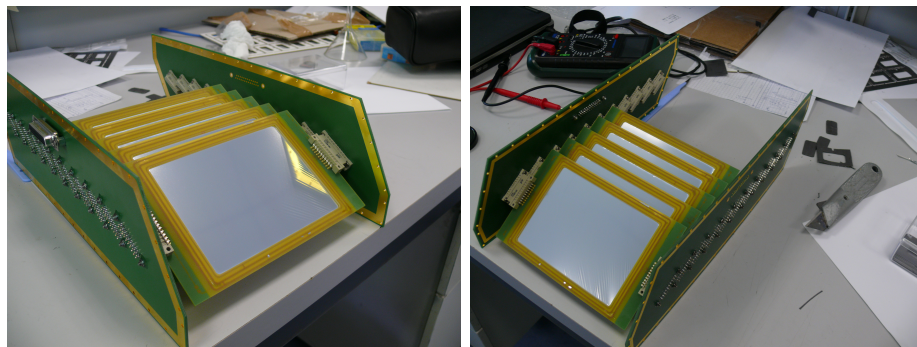

Figure 3.3: Detector without the aluminium housing. Only the side panel and electrodes are mounted together. The left side panel on the left picture is the signal output while the other side is a full ground plane.

All conducting paths which provide output signals are on the inner surface and directly connected to a 25-pin sub-D connector.
In figure 3.2 the connectors for the electrodes at a tilted angle of 60° with a distance of 2.4 cm to the next connector are shown. The used connector [5] consists of 20 pins [6] and a guided

---

[5] 102-80065 from ept company
[6] only one pin used for signal transport

housing which provides a good mechanical stability. Another advantage was the low force
to plug or unplug this connectors, because all 17 connectors on the second PCB have to be
plugged in simultaneously.

3.3.2   Frames of the Detector Foils

The frame of the detector foils are also made of PCB material with a rectangular shaped hole
in the middle. The 35 μm thick gold plated copper frames operate as a contact for the foil
but also as a guide for resin glue dispensed between the inner pair of them. To put on the
glue onto the foil frames an hallow needle and a automatic pressurized gun was used. This
allows to apply a rather constant amount of glue per unit length. Even so the x,y motion of
the cartridge was done manually.
To connect the frame with the side panel and provide the mechanical precision, the 2 connectors[6]
are mounted on the left and right side as pictures in figure 3.4.

Figure 3.4: Frame without any components

To prevent two different PCBs, one for GND and the other for VCC, a variable jumper was
used, that could be connected to different pins at the plug. These are pictured in figure 3.4
on the right side of the picture.
The bottom layer of the PCB has no additional function.

3.4   Detector Foils

The layout of the electrodes needs the frames discussed in the previous section covered with
a conducting layer. The conducting layer is composed of 2 μm Mylar$^{®}$ foil metallised with a
nanometer thick layer of aluminium on both sides. Advantages of this foil are good mechanical
stability, even if it is very thin, so that the deposited energy of the ions is as low as possibly.
For the covering of the PCB and providing a contact to the foils several steps were necessary.
First of all the Mylar$^{®}$ was stretched on a larger plastic frame. Thus the area in the middle
was free flying and flat. Two component epoxy glue was put on in a very thin band between
the two inner contact frames of the PCB foil frame. After that the PCB got dropped upside
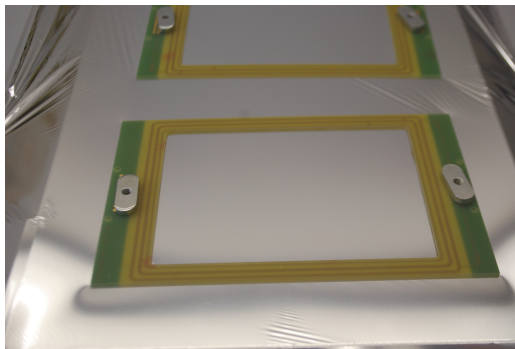down on to the foil.

Figure 3.5: Tensioned foil with frames on it

After the glue got dry, the setup was turned around and the foil got cut along the outermost contact frame with a soldering gun. Since it is necessary for the operation to connect both sides of the foils with a conductive glue, this method conductive an area were the glue could be put on and connect the foils electrical to the contact frame. Since the conductive glue is expensive only a small area got covered with it. The rest of the cutting edge got fixed with normal epoxy resin adhesive to avoid sharp edges of electrodes in the gas volume.
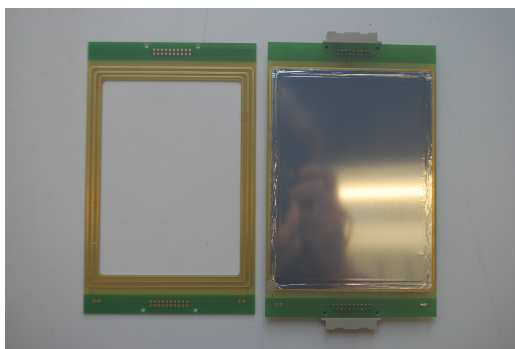In a final step the two connectors and the jumper were soldered to the board.

Figure 3.6: on the left a "naked" and on the right a covered PCB

To prevent the foils from being damaged during the assembling difficulties occurred. The frames had sharp edges that needed to be smoothed before and to prevent them from slicing the foil.

3.5   Acquisition Electronics

To minimize cable attenuation and capacity the pre-amplifier was diretcly fixed on top of the detector housing. For collecting the charges accumulated on the five detector foils, a charge sensitive pre-amplifier [7] was used with a range of 2.5 MeV Silicon equivalent and a decay time of 30 μs. The differential outputs of the preamplifier were fed into a 16 channel shaping amplifier with timing filter and constant fraction discriminator. [8].
The software of choice was Marabou. This is a combined data acquisition and online analysis software package with a graphical user interface. The advantages are live-based plots of the measured data and the possibility of an easy use calibration of the detector. In addition the programm is written in C^{++} to adapt the software for the personal needs.

---

[7]MPR-32 from Mesytech
[8]MSCF 16, Gain:12, threshold: 18, shaping:1, pz:180

Chapter 4

Detector Test Experiment with ^{7}Li Ions and Protons

The detector, designed for comparatively large signals produced by the passage of high energy heavy ions, could hardly be tested by typical β, γ or even α sources in the lab. Therefore a special test experiment for this detector was performed at the Tandem accelerator of the Maier-Leibnitz laboratory (MLL) in Garching using low energy proton and lithium beams.

Major goals of this test experiment were to show the principal operation of the detector concept and the typical signal shapes produced. Also the energy resolution of the segments and its position dependency should be investigated. Finally the rate dependence of the resolution should be determined over a whole range up to 10^6 particles per second.

4.1 Accelerator and Beam Properties

The accelerator in the MLL is an electrostatic Tandem Van-de-Graff accelerator. Particle energies E are roughly defined by $E = (Z + 1)eU$ where U is the so called terminal voltage and Z is the expected charge state of the accelerated ion. The main parts of the machine are a positively charged terminal, a negative ion source and a vacuum tube. It is a further development of the Van-de-Graaf accelerator, because it uses the terminal voltage two times what explains the name tandem-accelerator.

First negative ions are accelerated towards the positive terminal. There they hit a stripper foil, where they lose several electrons. After this the positive ions get pushed away from positively charged terminal. The maximum terminal voltage for the MLL is 15 mega volts, but typically 12 mega volts are achievable in a stable long term operation. [8, 14-16] In our case we used a terminal voltage of 10MV, which means protons can gain 20 MeV while to the heavier lithium ions that gain 40MeV. This principle is summarized in the Figure 4.1.
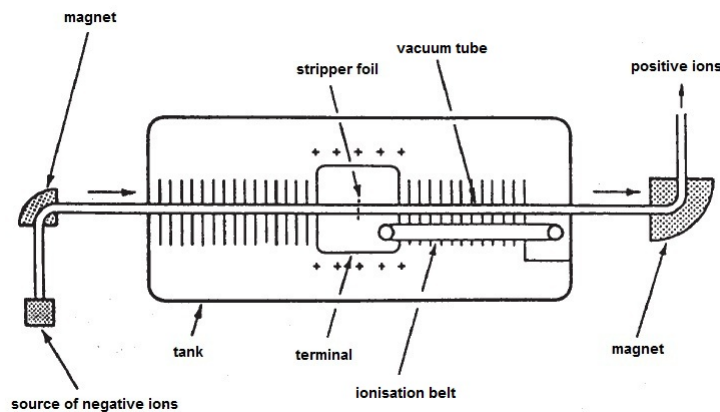
Figure 4.1: Schematic of a tandem accelerator [8]

Simply charged negative ions from the ion source (left side) reach the acceleration tank. Then they see the positive terminal and gain E=U · e. There they pass a thin Carbon foil [9] and get a positive charge state Z · e. Thus the terminal acts repulsive and they can gain another Z · e · U. The magnet (right side) separates the ion and charge state of interest.

In principle the ideal detector test would have been done with ions of energies E > 100 AMeV as e.g. available at the Gesellschaft für Schwerionenforschung (GSI) in Darmstadt. But the reason why it was made this way, is because there was no bigger accelerator with higher energies or ions available.

4.2   Experimental Setup

The beam was delivered in a vacuum tube into experimental Hall II to the beam line -10°. There it passes through a vacuum chamber that included the beam diagnostics. This chamber is usually used for proper detection test but our detector has to sit in air. The exit window of the vacuum chamber was a 50 μm thick Kapton foil, which provides mechanical stability even if its very thin.
For the device an adjustable table were needed to provide the right height for the incoming ions. If the ions get into the detector too low or too high, they might crash into the PCBs or side effects of the electrical field at the edges could reduce the amount of charge collected at the foil anodes.
To provide a good trigger signal in the proton experiment, an additional scintillator was used through a combination with another experiment. This scintillator was located directly behind the detector. To prevent damage to the front foil, the detector was placed 3 cm behind the exit window of the accelerator.
The supply of the detector gas P10 [10] was directly used from a bottle at quality 4.5.
The gas flow was adjusted [11] to flush the whole detector approximately twice per hour. A day before the experiment the device was purged with the detector gas, to minimize rest gas content. To supply the detector a voltage of U = 240V a NIM power supply [12] was used, in standard operation.
Figure 4.2 shows the experimental and figure 4.3 the electronic setup.

---

[9] $4 \frac{\mu g}{cm^2}$
[10] 90 % Argon, 10% CH_4 with 99.995 purity
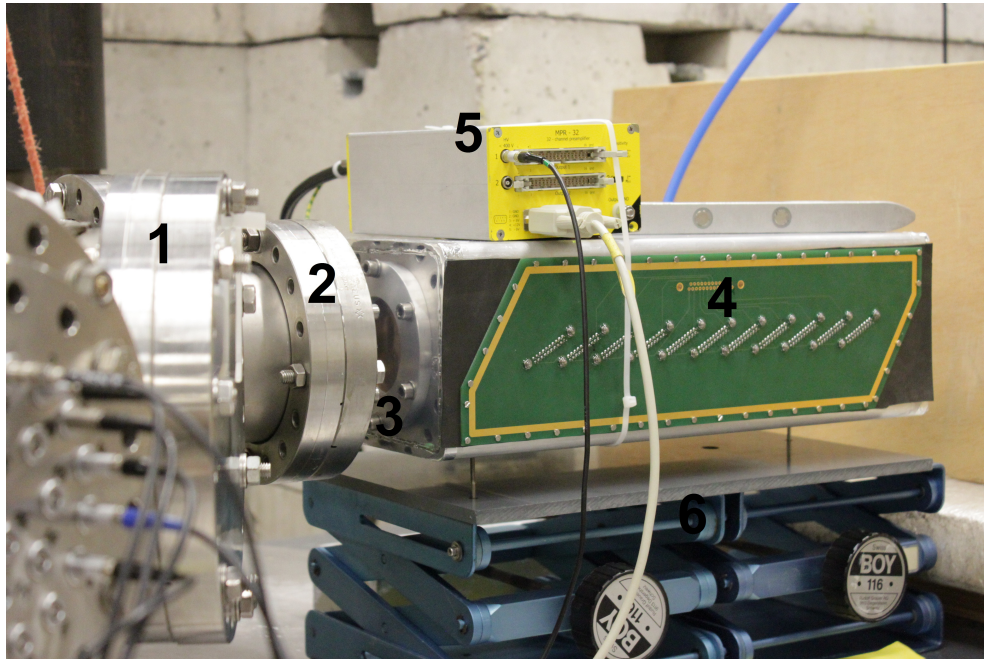[11] $25 \frac{l}{hour}$
[12] Mesytech MHV4

Figure 4.2: Experimental setup consists of: 1) the vacuum chamber, 2) window flange with 50μm Kapton window (can be seen as the detector entrance reflects very good), 3) small air gap (3cm), 4) detector, 5) pre-amplifier, 6)adjustable tables (XY $\pm$ 5 cm)
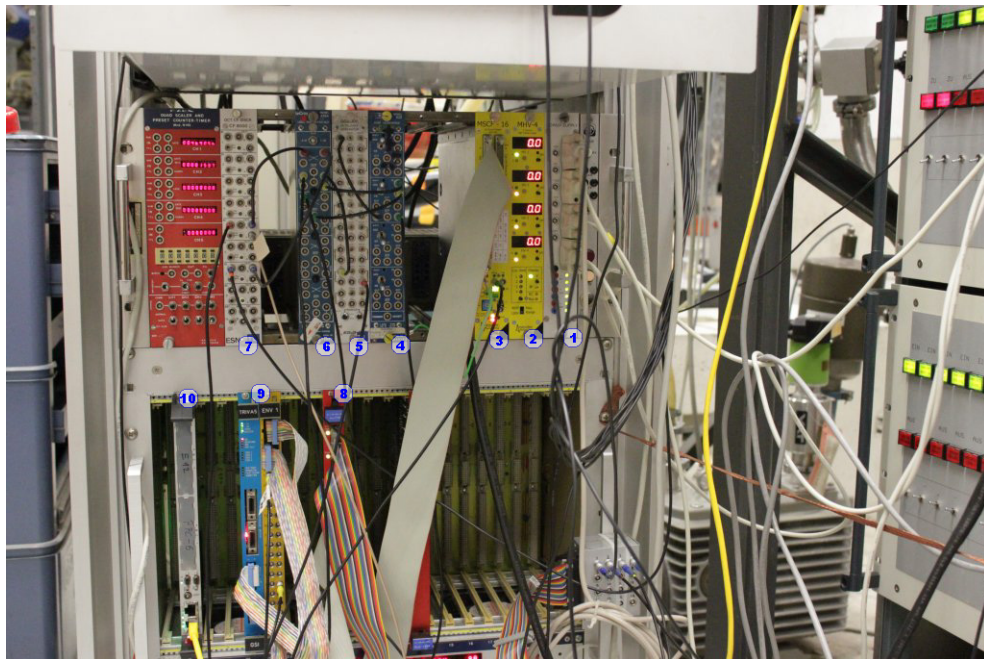

Figure 4.3: Electronics setup: 1)Low-voltage power unit for the pre-amp, 2)High-voltage power supply for the detector, 3)Amplifier MSCF 16, 4)Quad coincidence VME controller, 5)Gate generator, 6) Logic fan-in / fan-out, 7)Discriminator 8)ADC, 9)Trigger Module

4.3 Analysis of the Data

In this sections the data analysis and the results of the experiment at the MLL are discussed. To provide an easy understanding of the results a schematic sketch of the detector is illustrated in figure 4.3 which labels the anodes and the different detector gas cells. Each of the 5 anode signals is recorded in a raw adc histogramm as e.g. shown in figure 4.5.
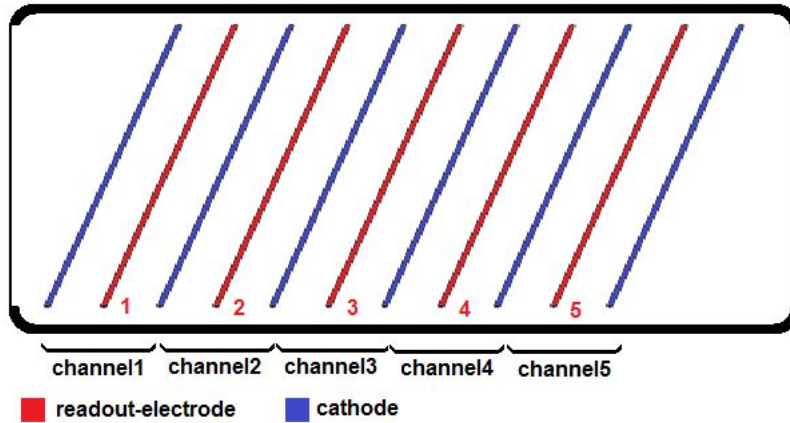

Figure 4.4: Schematic sketch that provides labels for the anodes and the detector gas cells. The beam enters from the left side.

First of all, each segment of the detector needs to be calibrated. For this the zero energy peak and the peak of the deposited energy were fitted with a Gauss-function for each channel. To relate the other channel with its energy, the loss of the ion was calculated theoretically with the program atima.[9] The entire spreadsheet with all energy loses and assumption can be found in the attachment A.1.
With this method, no pulser calibration was needed which was not possible in the short period the electronics was available. The calculated ΔE were compared to the measured average amplitudes to derive absolute values.
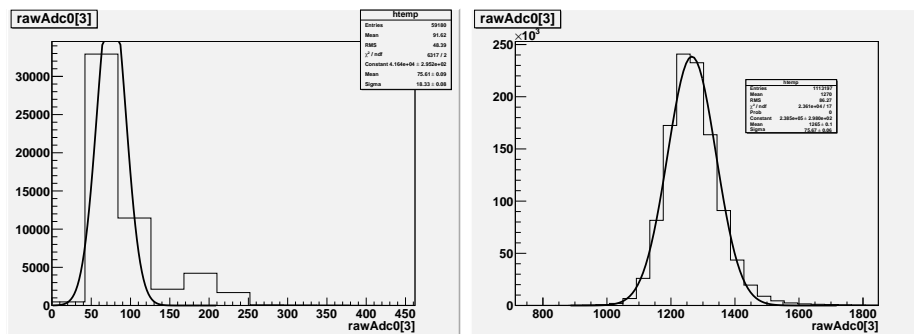

Figure 4.5: Calibration histogram of Channel 2. Random triggers produce the virtual zero peak (left) while channel 1270 represents the expected energy loss of ^{7} Li ions in this detector cell. Here Channel 1270 is related to the energy 5.93 MeV.

In figure 4.5 a calibration of one channel is illustrated. Here the channel 1270 is related to the energy 5.93 MeV.

4.3.1   Rate Dependence

As the detector is designed for high rate ion experiments the rate dependence of the final device is a very important topic that needs to be discussed.

Figure 4.6 illustrate energy loss measured for the lithium ions of the first four channels at an ion rate of 3 kHz. As shown the width of the peak gets bigger the more distance the incident ion is travelling. This is because of inelastic collisions where they lose energy or elastic collisions where the direction of motion gets changed and therefore the ionisation path is no more equal in every gas cell. Another reason is the statistical energy straggling [13] in the detector. But the most important effect which is broadening the peaks is a geometrical one. Due to the tilted foils the energy of each particle reaching a certain cell strongly depends on the vertical position which is not known in this experiment.
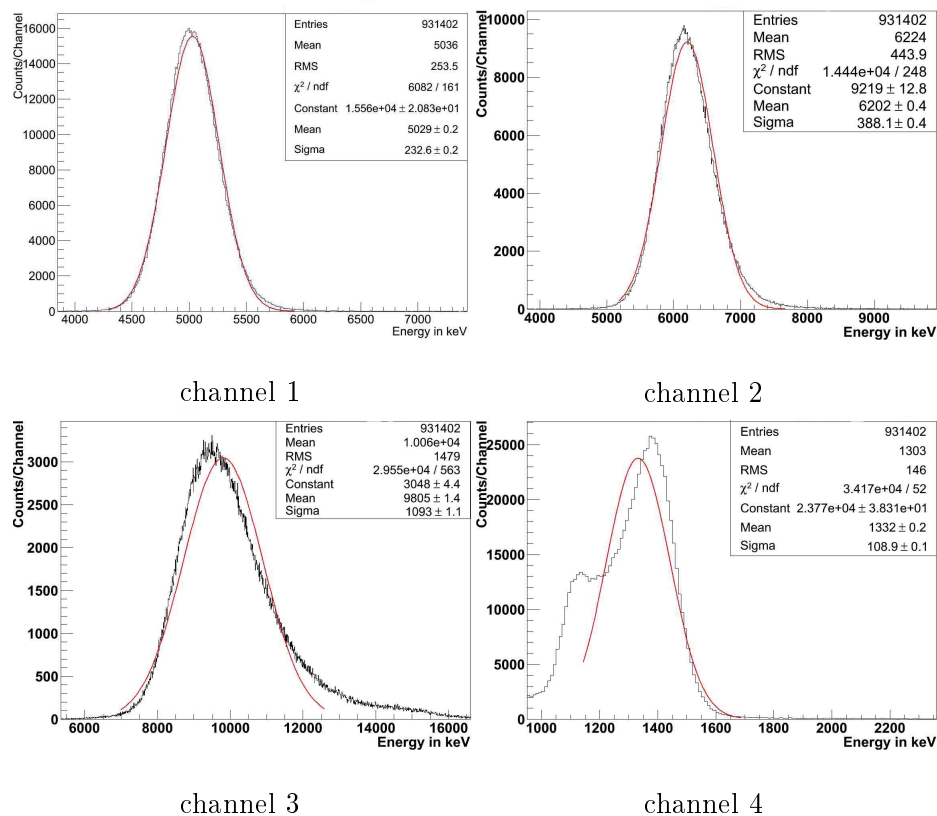

channel 1   channel 2

channel 3   channel 4

Figure 4.6: all four channels at 3kHz

As the readout of the deposited energy of the incident ion is segmented, it is possible to observe approximately the pathway of the Bragg curve. Comparing channel 1 and channel 2 the deposited energy increases slightly in consistence with the discussed curve in figure 2.1. The maximum energy loss was measured in channel 3 what implies that here the Bragg peak is observable. After the Bragg peak the deposited energy decreases, what is illustrated in the histogram of channel 4. The two peaks of this histogram will be discussed later.

To investigate the rate stability for every single channel of the detector these peak widths were measured over a whole ion rate range from 3 kHz to 120 kHz and the relative width are

---

[13]statistically varies around the average energy loss per length

illustrated in figure 4.7. Theses number were determined by the fraction of the σ[14] and the mean of the Gaussian fit.
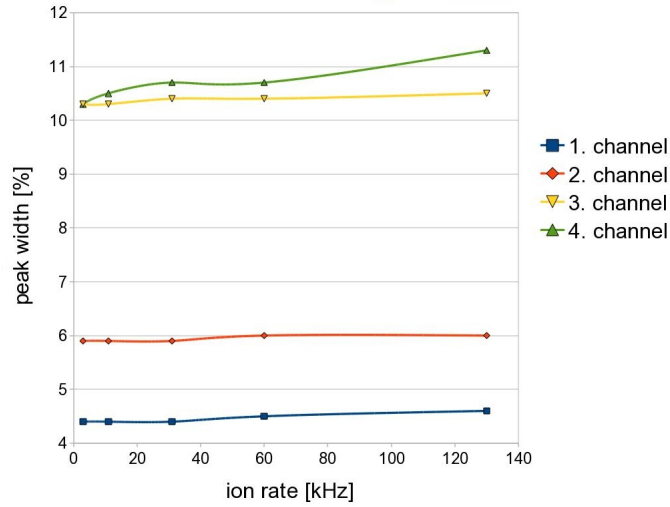

Figure 4.7: relative peak width of channel one to four at different ion rates

As a significant result the peak width of each channel changes barely over the whole measured range what implies a good rate stability.

Another important number in high rate experiments is the fraction of the pile-up events. This amplitude accrues when two or more ions are measured at the same time and saved as one event. A faster detector can resolve a higher rate of ionising particles without detecting two or more at the same time and therefore the relative amplitude of the pile-up is less than in a slower detector. Figure 4.8 shows the readout of channel two for 3 kHz and 130 kHz with a logarithmic scale.
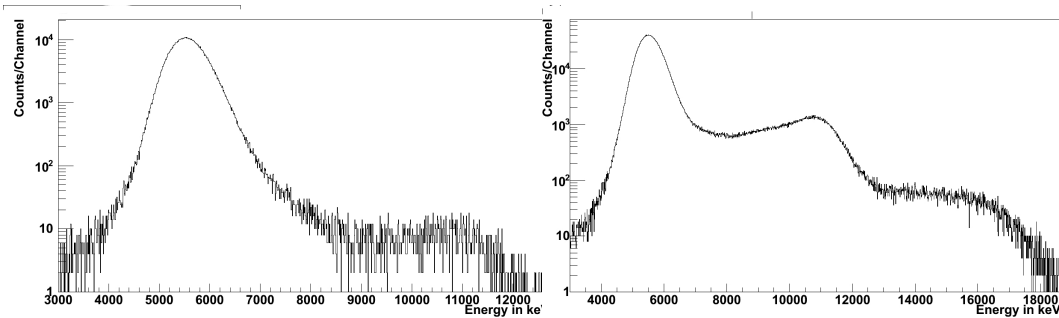
Figure 4.8: In the left picture the pile-up for channel two at 3 kHz is illustrated. On the right picture the pile-up for the same channel at 130 kHz. Both y-axis are with a logarithmic scale.

As sketched in figure 4.8 on the right side the pile-up for the 3 kHz run is very low, what makes a relative ratio of 0.22% to the original one. In comparison the pile-up ratio in the right picture for the 130kHz run increases significantly to a value of 3.79 %. Additionally there is also a second pile-up peak noticeable, what implies that three ions where measured at one event. As the value for the pile-up is constant in every channel for the same ion rate, this is also the value for the other three histograms.

---

[14]FWHM=2.35σ

These numbers also support the rate-stability of the detector, as the relative amplitude increases sparely even if the ion rate gets increase over an order of magnitude.

4.3.2 Energy resolution

To understand the problem how to derive an energy resolution from the experimental data taken with the ^{7}Li beam the sketch in figure 4.9 shows the schematic profile of the lithium beam. As it leaves the vacuum tube the beam is not perfectly parallel and gets more defocused as it travels through several layers of Maylor and gas undergoing collisions and straggling. Because of this effect the effective length that an ion travels and therefore the deposited energy varies for different ions.
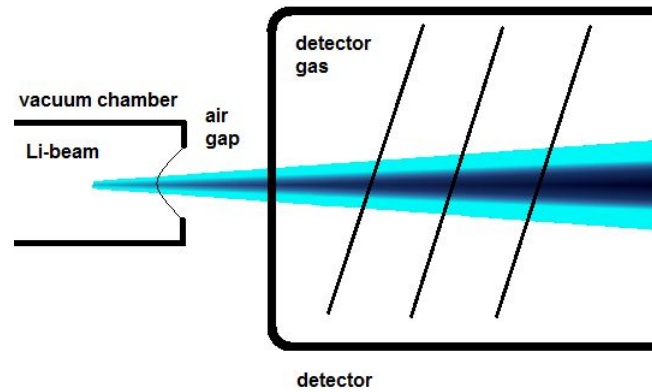
Figure 4.9: Schematic profile of the lithium beam as it travels through the detector. Because of collisions and straggling the beam gets defocused.

The measured spectra in figure 4.10 shows a Δ E-E_{res} diagram where the energy loss of channel three (y-axis) is plotted vs the energy loss of channel two (x-axis). The colours (z-axis) representing number of events of the measured data on a logarithmic scale.

Figure 4.10: Δ E - E_{res} plot of channel three vs channel two at 3 kHz

In the red area at number one where the most particles were detected the ion lost the calculated energy. This means that the deposited energy of channel two and the deposited energy of channel three matches the theoretical values for the incoming ion. This is also a clear correlation, as the increase of the energy loss in channel two results in an increase of the energy loss in channel three. 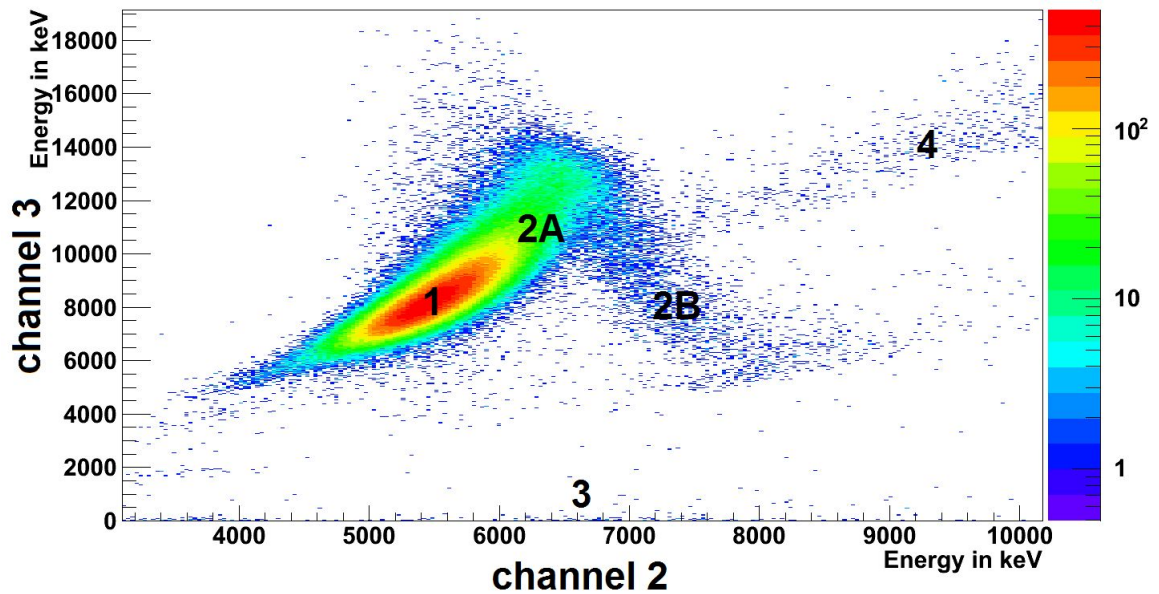These measured particles are able to pass through both channels and procuding a furhter signal in the following channels.

Area number 2A in the figure represents particles that energy losses is over the calculated values in both channels. The reason for this increased energy loss could be a elongated ionisation path through the gas cells based on energy straggling.

The area at number 2B shows a clear anti-correlation as a increasing energy loss in channel two is related to a decreasing energy loss in channel three. This implies that the velocity in channel two is relatively small and therefore the energy loss is very high. Then they get stopped in channel 3 and deposit their remaining energy.

As it is possible that some ions didn't even reach the third channel and are stopped behind the second one, there are also counts at number three. This is visually as the ions at the bottom of the y-axis made a signal in channel two but the measured signal for channel three is nearly zero.

In this figure there also a tiny pile-up can be distinguished at the area four, as this energy loss is very high and unlikely for a single ionising particle.

Looking into the fourth segment the data get even more interesting. Figure 4.11 illustrates the remaining energy of channel four (y-axis) versus the sum of the energy loss from channel one to three (x-axis) where all ions where stopped. So the sum of the points coordinates is related to the whole amount of deposited energy, as in channel five no left energy were measured.
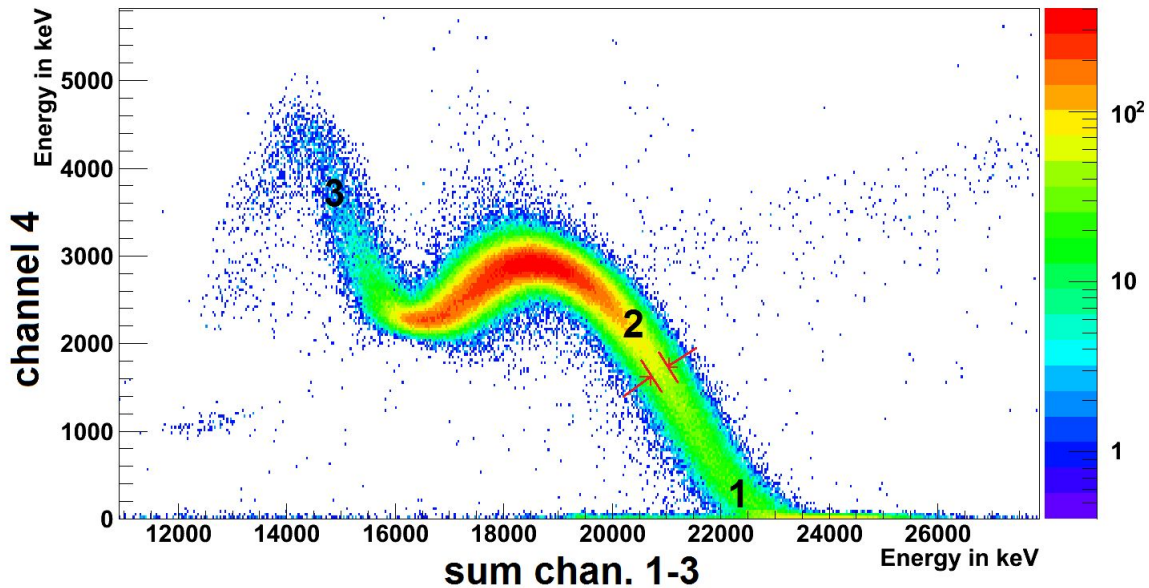
Figure 4.11: E_{res}-Δ E plot for the sum of channel 4 plotted against channel 1-3 with logarithmic z-scale

This plot illustrates the position where the ion was stopped and related to this point where the maximum of the energy loss took place (Bragg-peak).

In area number one in the figure there are several ions with no energy deposit measured in the fourth channel. This signifies that these ions have lost all their energy in channel one to three and were stopped before they could reach the fourth channel. The approximately mean energy

loss for this ions is 23 MeV, what is nearly the whole calculated deposited energy loss for all four channels with value of 22.24 MeV. This is explainable through the internal calibration which only takes into account the "ideal" particles of constant penetration depth. This also produces as a result a non constant total energy of the particles and has to be understood by a more detailed simulation.

The number two in the figure represents ions that made a signal in channel four and were stopped before the readout-electrode four. This could be found out with a comparison of number three in the picture. The local minimum implies that energy is "missing", what is a hint that these ions lost this energy as they passing through the fourth readout-electrode. As no signal was measured in channel five the approximately stop position of the ions is known. Another important aspect of this figure is, that it gives the possibility to determine the energy resolution of the detector for each channel. The resolution is related to the width of the S-type graph, what is approximately 0.15 MeV at the marked spot in the figure. This number matches perfectly the amount of energy-straggling with a calculated value of 0.217 MeV for e.g ions with 28 MeV kinetic energy passing through 24 $\frac{mg}{cm^2}$ material. All assumptions of this with atima [9] calculated value can be found in the attachment A.2. This implies that the resolution of the detector is limited by the experimental setup.

4.3.3 Position Depence

In this experiment the relation between position of the intruding beam an the measured output signal of the final device was investigated. In a different run a proton beam of 20 MeV kinetic energy and a rate of 300 Hz. Compared to lithium the protons should provide a rather constant energy loss signal in all segments as there is a relatively small energy loss on the different dead layers. First a control run near the detector center was recorded and then the detector was displaced, once in horizontal and in vertical direction to investigate the effects of proton dependent amplitudes.

Figure 4.12 shows the schematic layout of the different positions where the ion beam entered the detector and the resulting signal was measured.
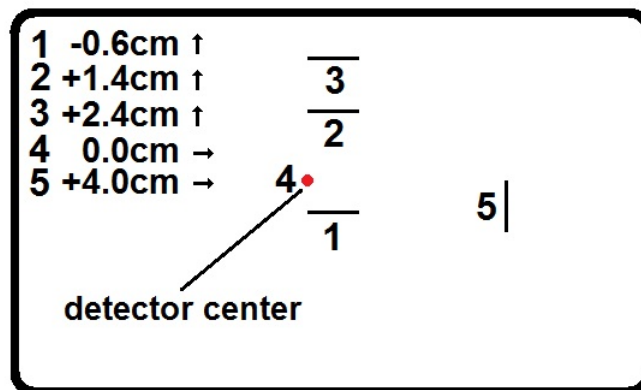
Figure 4.12: Schematic layout of the position dependence test. Every single number is related to a test run at a different detector position.

As the deposited energy of the protons [15] in every channel was nearly the same and the results showed no difference for a single run only channel 5 gets illustrated. In addition the illustrated figures are not calibrated, as only the effect of the displacement is investigated and so the raw

---

[15]0.16 MeV

data of the ADC are shown.

Figure 4.13 illustrates the results for the vertical test. The height of the detector related to the beam was changed in one cm steps by adjust the table height.
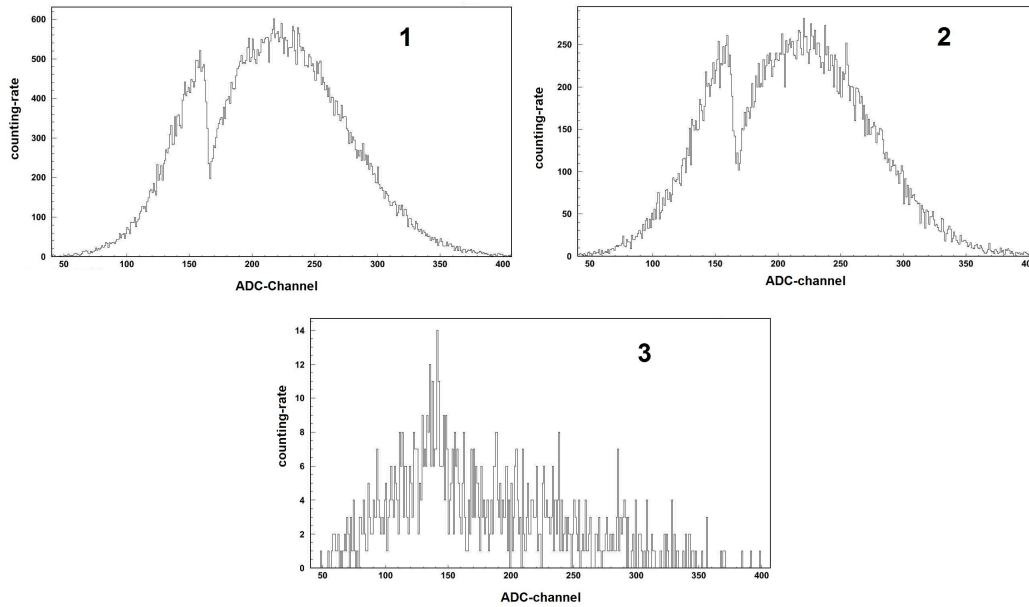

Figure 4.13: Results for the vertical test. The last picture shows the effect when the beam hits the PCB

The first peak around the ADC channel 150 has no physical relevance as it is the zero peak. The second peak is the signal of the protons as they flying through the detector.

Picture one in the figure shows the control run nearby [16] the middle point as a reference. The second picture illustrates the measured data at 1.4 cm above the middle point. This is the last position where no effect were observable. Already at 2.4 cm above the detector middle point no more signal were collected with the plastic scintillator behind the chamber which is a clear indicator that particles were no more passing through the foil area.

As the distance from the middle point for the measurement in the third picture is only approximately known only a minimum estimation of 1 cm from the PCB frame is possible where no effects of the displacement will occur. This equals 2.8 cm of active area.

The next test run was performed in horizontal position and the results are illustrated in figure 4.14.

---

[16]0.5 cm above
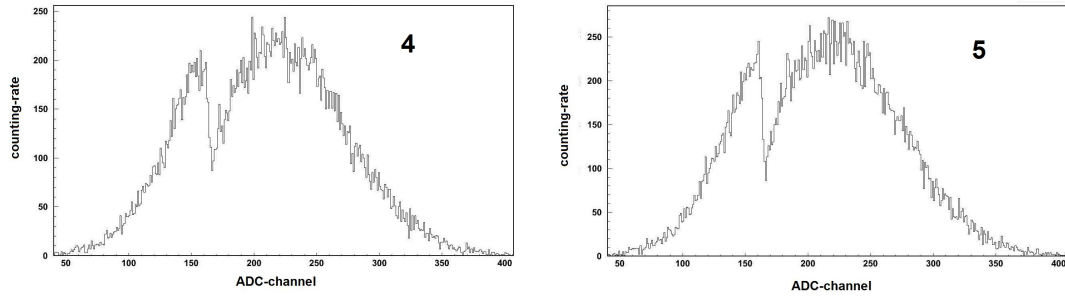
Figure 4.14: Results for the horizontal test. The first picture is the control run.

Due to insufficient measurements, the point where the displacement effects took impact couldn't be investigated. Therefore only a approximation is possible, that a displacement of 4 cm from the middle point has no impact of the measured signal as this was the farthest distance from the middle point that was recorded and illustrated in the second picture. So an aktive area of a minimum value of 8 cm could be determined.

As a overall result a minimal active area of 22.4 cm^2 could be determined for the detector. In addition the test showed that it is even possible to detect protons at an average energy loss of 78 keV per segment only.

Chapter 5

Summary and Outlook

5.1 Summary

The basic mechanical layout of the Tilted-Electrode-Gas-Ionisation-Chamber develop in the framework of this thesis is as a very variable structure. The design allowed free selectable angles and a high mechanical preciseness. The precision that is necessary to resolve two ions differing by one atomic number Z could be easily achieved through the PCB architecture and segmentation.
Also the gas tightness for a reliable measurement, can be provided through the ready-made aluminium case and the mounted PCB with sealing-layer.
In the experimental test at the MLL-accelerator the detector-device proved the concept of functionality. As a result of the investigation of the rate dependence of the device the relative peak width for each channel was nearly independent over the whole range of tested ion rates (3 kHz - 130 kHz). Additionally even at high rate experiments the relative fraction of the measured pile-up never exceeded 4 %.

Through analysis of the ΔE-E_{res} plots for the 40 MeV lithium beam, it was possible to approximately identify the point where the ions where stopped in the detector. Even so it is hard to define a charge resolution ΔZ with such low energy ions. Using a ΔE-E_{res} plot it was possible to measure the absolute energy resolution which was in the range of 150keV/segment. This value is still close to the limit caused by the energy-straggling of the incident ions and therefore limited by the experiment setup. In the real application using much higher energy ions the resolution might be still much better.

5.2 Outlook

As the detector is designed for heavy ions with high energies, an experiment at different accelerator would be reasonable to study the properties of the detector at higher energies and with different ions. In this way it also would be possible to test the detector with different tilting angles (e.g. 30°) of the electrodes or attempt various detector-gas-mixtures, to investigate differences in the results. Using CF_4 as a much faster detector gas would improve the rate limits significantly. [10, S.3] Especially the angle is of peculiar interest. Due to this angle it would be possible to add more electrodes to make the detector even faster. But this also means an increase of the number of readout channels. Connecting several of these channels as e.g. shown in figure 2.5 might help to optimize the signal to noise to reach the best compromise of speed and resolution.
To improve further a tracking system for the trajectory of the incoming ionising particle could

be build. This might be constructed through segmented electrodes by a PCB, so no new casing has to be designed and only the current one has to be improved. If only a certain energy loss is desired a complete modular construction could be build, variable in the length of the housing and therefore the ionising length.

Appendix A

attachment

A.1   energy loss table

Sheet2

Energy Loss

assumptions:

material	charge [e]	mass [u]	density [g/cm^3]
Li (40 MeV)	3	7	
H (20 MeV)	1	1	
Air	7	15	1.1985*10^-3
Kapton&Mylar	5	10	1.42
Ar90-Methan10	16	32	1.4758*10^-3

enery loss was calculated with atima

layer	material thick. [mg/cm^2]	Lithium: energy loss [MeV]	Hydrogen: energy loss [MeV]
Kapton	7.1000	4.5420	0.1675
Air	3.5955	2.2000	0.0828
Mayler	0.2840	0.2020	0.0067
Gas	8.8548	5.1800	0.2245
1. foil (1)	0.5680	0.4700	0.0068
1.foil to 2.foil (1;2)	3.5428	2.3100	0.0775
2	0.5680	0.5110	0.0067
2;3	3.5428	2.5100	0.0778
3	0.5680	0.5660	0.0069
3;4	3.5428	2.7760	0.0780
4	0.5680	0.6420	0.0069
4;5	3.5428	3.1550	0.0783
5	0.5680	0.7560	0.0069
5;6	3.5428	3.7470	0.0786
6	0.5680	0.9580	0.0069
6;7	3.5428	4.9400	0.0789
7	0.5680	1.5100	0.0067
7;8	3.5428	2.8000	0.0791
8	0.5680		0.0070
8;9	3.5428		0.0794
9	0.5680		0.0070
9;10	3.5428		0.0797
10	0.5680		0.0070
10;11	3.5428		0.0800
	overall loss:	39.7750	1.3376

foil	channel	energy (Li)	energy (H)
2	1	4.82	0.16
4	2	5.93	0.16
6	3	8.69	0.16
8	4	2.8	0.16
10	5	0	0.16

A.2   Energy Straggling

Assumptions and results for the calculation of the energy straggling:
charge of fragment: 3
mass of fragment [amu]: 7.000000
energy of fragment [MeV/u]: 4.000000
charge of material: 20
mass of material: 40
material thickness [mg/cm2]: 24.000000

particle: Z=3 A=7.000 E=4.00000 MeV/u
target: Z=20 A=40 Thickness=24.000000 mg/cm2
exit energy : 1.137317 MeV/u
energy loss : 20.038783 MeV
energy straggling : 0.031510 MeV/u (SD)
range : 29.143820 mg/cm2 -> 5.143820 mg/cm2
range straggling : 0.175245 mg/cm2 (SD)
angular straggling : 50.776608 mrad

A.3   Mechanical-Variance

Derivation for the formula of the mechanical limits for the detector.
E deposited energy, c constant, l length, maximum Z atomic number.

$$E = c \cdot l \cdot Z^2 \tag{A.1}$$

$$\frac{dE}{dl} = c \cdot Z^2 \rightarrow dE = c \cdot Z^2 \cdot dl \tag{A.2}$$

$$\frac{dE}{dz} = 2 \cdot Z \cdot l \cdot c \rightarrow \frac{Z}{dZ} = 2 \cdot \frac{l}{dl} \tag{A.3}$$

$$\frac{\Delta l}{l} = 2 \cdot \frac{\Delta Z}{Z} \tag{A.4}$$

With Z=100, l=6cm, ΔZ=1 $\rightarrow \Delta l = 0,12 cm$

A.4   Pulse Formation

Derivation of the pulse formation function V(t). The schematic layout of the detector is illustrated in figure 2.4.1
E=electric field, Q=charge on chamber plates, dQ$^+$, dQ$^-$=changes in the positive and negative charge, $V_0 = $ applied voltage, V(t)=voltage accros the resistor (signal), ω^+,$\omega^- = $ drift velocoty of the positive and negative ion, T$^+$, T$^-$ time that the ion or electron needs to reach the plate.

electric force times distance = change electrostatic energy

$$eE(dx^+ + dx^-) = d\frac{Q^2}{2C} = \frac{Q}{C}dQ \approx V_0\left(dQ^- + dQ^+\right)$$

For the last step the assumption was made that dQ is so small that V_0 doen't change

The voltage accros the resistor is given by:

$$V(t) = \frac{1}{C}\int\limits_0^t dQ(t) = \frac{1}{C}\int\limits_0^t (dQ^+ + dQ^-)$$

$$\rightarrow V(t) = \frac{1}{C}\int\limits_0^t \frac{e}{V_0}E(dx^+ - dx^-)$$

For a plate chamber the applied eletric field is constant and therefore the drift velocity

$$\rightarrow V(t) = \frac{e}{Cd}\int\limits_0^t (\omega^+ + \omega^-)dt = -\frac{e}{Cd}(\omega^- t + \omega^+ t)$$

Bibliography

[1] K. Kimura, T. Izumikawa, "High-rate particle identification of high-energy heavy ions using a tilted electrode gas ionization chamber," *http://www.sciencedirect.com/science/article/pii/S0168900204019953*, 2003.

[2] Nicholas Tsoulfanidis, Sheldon Landsberger, *Measurement and Detection of Radiation*, vol. 3. CRC Press, 2011.

[3] W. Blum, W. Riegler, L. Rolandi, *Particle Detection with Drift Chambers*, vol. 2. Springer, 2008.

[4] Wikipedia, "Wikipedia: Bragg Curve," *http://en.wikipedia.org/wiki/Bragg_peak*, 2012.

[5] Glenn F. Knoll, *Radiation Detection and Measurement*. Wiley, 2010.

[6] Jaakko Julin, "Development of a High Energy Resolution Gas Ionization Detector for a Recoil Spectrometer," *https://jyx.jyu.fi/dspace/bitstream/handle/123456789/37404/URN:NBN:fi:jyu-201202191212.pdf?sequence=1*, 2011.

[7] Andreas Stolz, "Untersuchung des Gamov-Teller-Zerfalls in der Nachbarschaft von ^{100}Sn," June 2001.

[8] M. Weber, C. Herlitzius, "Schwerionenstreuexperiment am Tandembeschleuniger," *http://www.e12.physik.tu-muenchen.de/stud/fopra/schwerionen52/anleitung.pdf*, Apr 2010.

[9] Geissel, H. and Scheidenberger, C. and Malzacher, P and Kunzendorf, J and Weick, H, "atima: energy loss calculator," *GSI*, 2012.

[10] Dr. R. Schneider, Andreas Stolz , "Technical Manual - Ionisation Chamber MUSIC80," *http://www-w2k.gsi.de/frs/technical/FRSsetup/detectors/music80/music80_manual.pdf*.

Acknowledgement

First of all I would like to thank Prof. Dr. Walter Henning for the opportunity, to write my bachelor thesis at the professorship E12 of the TUM.

I would like to thank especially my scientific supervisor Dr. R. Gernhäuser. He always showed a lot of patient, even if I didn't understand a problem immediately. He gave me the opportunity to learn much in physics and other fields of modern research.
Also I would like to thank all the employees of the professorship. Not only for the support, but also for the pleasant working atmosphere.

In the end I would like to say thanks to the E12 coffee machine. No matter what time it was, the machine helped through a period of tiredness. And of course to Patrick Remmels for the nice coffee breaks.